Simple model for structural properties and crystal stability of *sp*-bonded solids

J. A. Majewski
Institut für Theoretische Physik, Universität Graz, A-8010 Graz, Austria
*and Institute of Physics, Polish Academy of Sciences, PL-02-668 Warsaw, Poland**

P. Vogl
Center for Nonlinear Studies, Los Alamos National Laboratory, Los Alamos, New Mexico 87545
*and Institut für Theoretische Physik, Universität Graz, A-8010 Graz, Austria**

(Received 17 November 1986)

A simple, universal model for structural properties of *sp*-bonded semiconductors and insulators is presented. The model elucidates the physical mechanisms determining the chemical trends and predicts semiquantitatively the stable crystal structures, bond lengths, bulk moduli, transition pressures of structural phase transformations, long-wavelength transverse optical phonons, and band structures for binary nonmetals in the rocksalt, cesium chloride, and zinc-blende phases. The theory explains the puzzling strong cation and weak anion dependence of the observed structural transition pressures. It predicts, as a function of pressure, a universal sequence of structural phase transformations among the cubic phases of binary solids. A drastic softening of the transverse optical phonons across the pressure-induced phase transition from the zinc-blende to the rocksalt structure in II-VI compounds is also predicted. The physical origin of this softening is shown to be closely related to ferroelectricity. It is shown that the chemical trends in the structural properties of semiconductors *and* insulators are governed by a counterbalance of attractive and repulsive short-range interactions, whereas long-range interactions play only a minor role, in contrast to the classical point-charge models of ionic crystals. The theory is based on the semiempirical tight-binding method and includes charge transfer and nonorthogonality effects. Only properties of the neutral atoms are used as input for a given crystal. The total energy is explicitly minimized as a function of volume in order to find the static and dynamic equilibrium crystal properties.

I. INTRODUCTION

The study of cohesive properties and structural phase transformations of insulators and semiconductors is one of the classic problems in solid state physics.[1–4] Most of the models which have been developed so far are phenomenological.[2,3,5–9] These models are often applicable only to a restricted class of solids and have little predictive power. Conversely, first-principles methods have been developed in the last ten years which permit the calculation of the cohesive properties of a variety of solids with often a high degree of accuracy.[10,11] Yet these computationally elaborate techniques do not easily provide insight into the dominant physical mechanisms. Therefore, presently there is a substantial interest in new approaches which provide a link between the full-scale microscopic, quantum mechanical calculations of structural stabilities and the intuitive physical and chemical arguments.[4,12–18]

It is the purpose of this paper to provide such a link by presenting a simple yet realistic and universal semiempirical tight-binding model which is able to predict the chemical trends in a variety of static and dynamic structural properties of a broad class of nonmetals. An important aspect of this method is that it does not discriminate between "covalent" and "ionic" solids but treats both on an equal footing.

It is widely believed that a prediction of the relative stability of two crystal structures, which usually differ by an energy of the order of 0.1 eV, requires an extremely accurate theory. Indeed, the state-of-the-art *ab initio* methods for structural properties, which are based on elaborate density-functional calculations,[10,11,19–26] or the Hartree-Fock method,[27] are by now very well suited to answer specific questions quantitatively.[25,26,28]

On the other hand, several empirical models uncovered clear chemical trends in the structural stabilities of solids[2,3,5–9,29] and suggest that the key for predicting *and* conceptual understanding the relative structural energies of solids is not absolute accuracy but a model which carefully incorporates the chemical trends in the *atomic* characteristics.

The oldest and most widely used empirical model of cohesive properties and structural stabilities of insulators are the Born's model and its extensions.[2,6–8] These models incorporate many of the intuitive chemical arguments of Pauling[1] but are restricted to ionic solids and require many empirical parameters to obtain semiquantitative results (e.g., 18 parameters in 20 crystals;[8] see also Ref. 30 for a critical discussion). In addition, this model draws heavily on the concept of a static effective ionic charge which may vary by as much as $\frac{1}{2}$ electron even in "classical" ionic solids such as NaCl depending on the method employed in its definition.[29,31,32]

Phillips and Van Vechten[3,5] were able to successfully order the relative stability of tetrahedral structures with their well-known concept of ionicity which is based on the

dielectric properties of solids. This approach and closely related phenomenological models have been used to obtain structural maps which provide an intriguing overall classification of solids in terms of various types of core radii.[9] However, they do not shed light on the origin of the different regions of structural stability.

Since the first-principles calculations, including the approximate electron-gas models,[33–35] seem not well suited to provide a conceptual framework for understanding chemical trends in the static and dynamic structural properties of a broad class of nonmetallic solids, recently several authors have developed theoretical schemes which can provide a link between accurate calculations and a physical understanding of the data.[4,12–17,36–38] Andersen and Jepsen[13] have developed a rigorous scheme to put the linear muffin-tin-orbital method into the framework of a tight-binding model. Chelikowski and Burdett[14] confirmed qualitative predictions of Phillips concerning transition pressures from tetrahedral to octahedral structures of semiconductors. They augmented the *ab initio* potential of GaAs by a localized model potential to simulate trends with ionicity. Harrison and others[4,15–17,36–38] have developed a modern version of the empirical tight-binding method for the electronic structure of solids. Formally, this approach follows closely the *ab initio* methods by expressing the total energy in terms of Hamiltonian matrix elements. The crucial simplification is that these solid-state matrix elements are determined approximately by scaling arguments and by incorporating the chemical trends in the atomic data rather than being calculated. So far, the tight-binding approach was applied to relative structural stabilities of bulk crystals only in the case of *pd* metals.[12]

In the present paper, we shall make use of the tight-binding method and develop a universal and predictive model which allows a physically transparent understanding of the chemical trends in structural properties and relative phase stabilities of semiconductors and insulators. We shall present results for cubic binary compounds. The theory is based on a microscopic total energy minimization procedure and requires only properties of the isolated atoms as empirical input.

This paper is organized as follows. In Sec. II we present the model. In Sec. III band structures and static structural properties, namely, equilibrium bond lengths, bulk moduli, relative phase stabilities, and transition pressures, are calculated for the rocksalt, the cesium chloride, and the zinc-blende phases of nonmetallic binary octet compounds. In addition, long-wavelength optical-phonon frequencies of several II-VI and IV-VI compounds in the zinc-blende and rocksalt phases are predicted. Since the present model is semi-empirical, it is imperative to check the influence of the various simplifications on the results. This is done in Sec. IV. The major purpose of the semiquantitative results in Sec. III is to support the new *qualitative* results concerning the structural stabilities of solids, presented in Sec. V. This section demonstrates the ability of the present approach to uncover and explain chemical trends in the data. Finally, we present a highly simplified but illustrative and analytical version of this theory in the Appendix.

II. THE MODEL

The total energy per unit cell of a solid, consisting of rigid ion cores and valence electrons, can be written in the form

$$E_{\rm tot}=\frac{1}{N}\sum_{n,\mathbf{k}}^{\rm occ}\varepsilon_{n\mathbf{k}}-E_{\text{el-el}}+E_{\text{core-core}}\ . \tag{2.1}$$

The first term on the right-hand side (rhs) of Eq. (2.1) is the band-structure energy per unit cell. It is obtained by solving the one-electron Schrödinger equation

$$H_{\rm el}\,|\,n,\mathbf{k}\rangle=\varepsilon_{n\mathbf{k}}\,|\,n,\mathbf{k}\rangle\ , \tag{2.2}$$

and summing over all occupied band states $|\,n,\mathbf{k}\rangle$. In Eq. (2.1), N is the number of unit cells in the crystal. The second and third term in Eq. (2.1) represent the electron-electron interaction between the valence electrons which is doubly counted in the first term and the core-core interaction, respectively.

In order to evaluate $E_{\rm tot}$, we generalize the empirical tight-binding method[15,39,40] and take into account long-range interactions. Only *sp*-bonded nonmetals will be considered in this paper. We exclude, therefore, a discussion of compounds with partially filled *d* or *f* states, although the present method can be adapted to this case.[41] The first step consists in solving Eq. (2.2). To this end, the wave function is expanded in terms of a minimal set of localized Lowdin functions,[39] consisting of a single *s* state and three *p* states per atom. The basis states on different atoms are not assumed to be orthogonal and will be orthogonalized explicitly as described below.

In the basis which results from the orthogonalization, the Hamiltonian matrix can be written as

$$H_{\rm el}=\sum_{\lambda,I}|\,\lambda,I\rangle\varepsilon_{\lambda I}\langle\lambda,I\,|\ +\sum_{\substack{\lambda,\lambda',I,I'\\(I\neq I')}}|\,\lambda,I\rangle \times t_{\lambda\lambda'}(\mathbf{R}_I-\mathbf{R}_{I'})\langle\lambda',I'\,|\ . \tag{2.3}$$

The basis states are labeled by the site I and the symmetry-related (collective) index $\lambda=(l,m)$, where l and m denote the appropriate angular-momentum quantum numbers. The two-center approximation is used for the offsite elements $t_{\lambda\lambda'}$. In addition, they are assumed to be nonzero only for the nearest and second-nearest neighbors and to follow Harrison's rule.[39] This gives

$$t_{lm,l'm}=\eta_{ll'm}\frac{\hbar^2}{md^2}\ , \tag{2.4}$$

where d is the distance between the atoms and $\eta_{ll'm}$ are universal constants. These constants couple the neighboring *s* and *p* anion (a) and cation (c) states and are taken from Ref. 42 for nearest neighbors. They are given by $\eta_{ss\sigma}=-1.38$, $\eta_{pp\sigma}=2.20$, $\eta_{pp\pi}=-0.55$, $\eta_{sapc\sigma}=1.68$, $\eta_{scpa\sigma}=1.92$. They were fitted in Ref. 42 to obtain adequate band structures for semiconductors. For next-nearest neighbors, we choose $\eta_{scsc\sigma}=-0.3$, and $\eta_{papa\sigma}=0.5$, as will be discussed in Sec. IV. The major effect of the latter matrix elements is to give an overall improvement of the calculated band structures; otherwise the coupling of second-nearest neighbors could be neglected.

For elemental semiconductors and insulators, the arithmetic average of the appropriate matrix elements is taken. The onsite Hamiltonian elements $\varepsilon_{\lambda I}$ in Eq. (2.3) are assumed to differ from free atomic-orbital energies by charge transfer effects and nonorthogonality corrections:[15,38]

$$\varepsilon_{\lambda I}=w_{\lambda I}-U_I(Z_I-Q_I)+\sum_{I'(\neq I)}(Z_{I'}-Q_{I'})V(\mathbf{R}_I-\mathbf{R}_{I'})+f_{\lambda I}\ . \tag{2.5}$$

Here, $w_{\lambda I}$ are the orbital energies of the free, neutral atoms which are given in Table I. U_I is an average of the intra-atomic two-electron Coulomb integrals of the valence electrons in the free atom of species I.[15] For the convenience of the reader, these values are also included in Table I. Z_I is the atomic number of the atom I and Q_I the total valence electron occupancy of this atom in the solid,

$$Q_I=\sum_\lambda Q_{\lambda I}=\sum_\lambda \frac{1}{N}\sum_{n,\mathbf{k}}^{\text{occ}} |\langle \lambda,I \mid n,\mathbf{k}\rangle|^2\ . \tag{2.6}$$

In Eq. (2.5), we assume $\varepsilon_{\lambda I}$ to vary linearly with occupancy, which corresponds to a Hartree approximation in the atomic case. The occupancies Q_I depend on the Hamiltonian matrix elements, in particular on $\varepsilon_{\lambda I}$, which in turn depend on Q_I. In the present model these occupancies are therefore calculated self-consistently in an iterative manner.

The third term on the rhs of Eq. (2.5) is the electrostatic inter-atomic potential at site $\mathbf{R}_I$ due to the other cores and electrons in the crystal. For large $|\mathbf{R}_I-\mathbf{R}_{I'}|$, V can be approximated by a Coulomb potential. We shall discuss modifications of V for small $|\mathbf{R}_I-\mathbf{R}_{I'}|$ later in this section.

The increase in the kinetic energy of the electrons upon compression of the solid is incorporated into this model by taking into account the nonorthogonality of the basis states.[4,16,38,39,44] It is this effect which prevents the collapse of the crystal in the present context. We approximately orthogonalize the localized basis functions to their neighbors by taking into account their overlap S to first order. This leads to the nonorthogonality correction $f_{\lambda I}$ in Eq. (2.5),[39]

$$f_{\lambda I}=-\tfrac{1}{2}(SH_{\text{el}}+H_{\text{el}}S)_{\lambda I,\lambda I}\ . \tag{2.7}$$

A similar correction affects also the off-diagonal matrix elements $t_{\lambda\lambda'}$ in Eq. (2.3). Since, however, their dependence on distance is constructed empirically, Eq. (2.4), the effect of the overlap S on $t_{\lambda\lambda'}$ is assumed to be already incorporated in Eq. (2.4).

Following extended Huckel theory[45] and Ref. 16, it is plausible to take the overlap matrix elements between atoms A and B to be proportional to the corresponding hopping matrix elements and inversely proportional to the atomic orbital energies:

$$S_{ll'm}=\eta_{ll'm}\frac{2}{K(w_{lA}+w_{l'B})}\frac{\hbar^2 r_0}{md^3}\ . \tag{2.8}$$

In Eq. (2.8), K is a numerical constant. Similarly to Ref. 16, we have taken a different value for K for each row of the Periodic Table and a geometric average for skew compounds. The values are $K_{\text{C}}=1.67$, $K_{\text{Si}}=1.31$,

TABLE I. Atomic term values for valence levels (Ref. 43) and intra-atomic Coulomb repulsions U (Ref. 15).

	Li	Be		B	C	N	O	F
$-w_s$ (eV)	5.39	8.41		13.46	19.19	25.71	33.85	42.77
$-w_p$ (eV)	1.04	2.55		8.43	11.79	15.44	17.19	19.86
U (eV)	8.17	10.25		10.26	11.76	13.15	14.47	15.75
	Na	Mg		Al	Si	P	S	Cl
$-w_s$ (eV)	5.14	6.88		10.70	14.68	18.94	23.92	29.18
$-w_p$ (eV)	0.53	1.26		5.71	8.08	10.65	11.90	13.77
U (eV)	6.17	7.28		6.63	7.64	8.57	9.45	10.30
	K	Ca	Zn	Ga	Ge	As	Se	Br
$-w_s$ (eV)	4.34	6.11	7.96	11.55	15.05	18.66	22.78	27.00
$-w_p$ (eV)	0.25	1.46	3.48	5.67	7.82	10.05	10.68	12.43
U (eV)	5.56	6.40	7.83	6.61	7.51	8.31	9.07	9.79
	Rb	Sr	Cd	In	Sn	Sb	Te	I
$-w_s$ (eV)	4.18	5.69	7.20	10.14	12.96	15.83	19.06	22.33
$-w_p$ (eV)	0.10	1.17	2.99	5.37	7.21	9.10	9.79	10.97
U (eV)	5.05	5.71	6.95	6.00	6.73	7.39	8.00	8.58
	Cs	Ba			Pb			
$-w_s$ (eV)	3.89	5.21			12.41			
$-w_p$ (eV)	0.10	0.96			6.95			
U (eV)	5.02	5.70			7.03			

$K_{Ge}=1.16$, $K_{Sn}=1.05$, $K_{Pb}=0.93$, respectively. These five values and the universal dependence of S on the distance between atoms A and B were fitted to obtain adequate overall agreement between the calculated and the experimental bond lengths and bulk moduli of semiconductors and insulators. The influence of these choices on the results is discussed in detail in Sec. IV. In Eq. (2.8), r_0 is an average valence state radius which enters the expression Eq. (2.8) for dimensional reasons, and is taken to be

$$r_0=\frac{e^2}{2}\left[\frac{1}{U_A}+\frac{1}{U_B}\right] . \tag{2.9}$$

Finally, we turn to the doubly counted electron-electron and the core-core energy in Eq. (2.1). Corresponding to Eq. (2.5), we split the electron-electron interaction into an intra- and inter-atomic term. In the Hartree approximation, the former is given by

$$E_{\text{el-el}}^{\text{intra}}=\frac{1}{N}\sum_I U_I Q_I^2 . \tag{2.10}$$

The remaining long-range terms in Eq. (2.1) can be lumped together and are given by

$$E_{\text{core-core}}-E_{\text{el-el}}^{\text{inter}}=\frac{1}{N}\sum_{\substack{I,I'\\(I\neq I')}}(Z_I Z_{I'}-Q_I Q_{I'})V(\mathbf{R}_I-\mathbf{R}_{I'}) . \tag{2.11}$$

The cohesive energy per unit cell, E_{coh}, is finally obtained by subtracting the total crystal energy, Eq. (2.1), from the energy of the isolated, neutral atoms.

So far, the derivation has been completely general and applies to any sp-bonded solid. In this paper, we apply this model to cubic, binary insulators and semiconductors. The three cubic phases which are of relevance for these solids are the rocksalt ($B1$), the cesium chloride ($B2$), and the zinc-blende ($B3$) structure. We shall henceforth label the two atoms per unit cell by an index i, where $i=a$ denotes the anion and $i=c$ the cation. In order to get transparent expressions, at first we assume the two-body potential V in Eqs. (2.5) and (2.11) to be strictly Coulombic for all $\mathbf{R}_I$ and introduce modifications afterwards. Then Eq. (2.5) reads

$$\varepsilon_{\lambda i}=w_{\lambda i}-(U_i-U_M)(Z_i-Q_i)+f_{\lambda i} , \tag{2.12}$$

with

$$U_M=\frac{e^2\alpha_M}{d} . \tag{2.13}$$

In Eq. (2.13), α_M is the Madelung constant which equals 1.7476, 1.7627, and 1.6381 for the rocksalt, cesium chloride, and zinc-blende structures, respectively. The overlap corrections to the diagonal matrix elements of H_{el}, Eq. (2.7), become

$$f_{si}=-n_{\text{NN}}(S_{ss\sigma}^{ii'}t_{ss\sigma}^{ii'}+S_{sp\sigma}^{ii'}t_{sp\sigma}^{ii'}) - n_{\text{NNN}}(S_{ss\sigma}^{ii}t_{ss\sigma}^{ii}+S_{sp\sigma}^{ii}t_{sp\sigma}^{ii}) , \tag{2.14}$$

$$f_{pi}=-n_{\text{NN}}\tfrac{1}{3}(S_{sp\sigma}^{ii'}t_{sp\sigma}^{ii'}+S_{pp\sigma}^{ii'}t_{pp\sigma}^{ii'}+2S_{pp\pi}^{ii'}t_{pp\pi}^{ii'}) - n_{\text{NNN}}\tfrac{1}{3}(S_{sp\sigma}^{ii}t_{sp\sigma}^{ii}+S_{pp\sigma}^{ii}t_{pp\sigma}^{ii}+2S_{pp\pi}^{ii}t_{pp\pi}^{ii}) , \tag{2.15}$$

where $i,i'=a,c$ and n_{NN} and n_{NNN} denote the number of nearest and next-nearest neighbors in the given structure, respectively. The electrostatic energies in Eq. (2.11) can be explicitly summed and give

$$E_{\text{core-core}}-E_{\text{el-el}}^{\text{inter}}=(Z_a Z_c-Q_a Q_c)U_M . \tag{2.16}$$

The total energy of the isolated neutral atoms $i=a,c$ in the unit cell is given by

$$E_{\text{atom}}=\sum_{\lambda i}Z_{\lambda i}w_{\lambda i}-\tfrac{1}{2}(U_a Z_a^2+U_c Z_c^2) , \tag{2.17}$$

where $Z_{\lambda i}$ is the number of valence electrons in the anion or cation valence electron shell of symmetry λ, and Z_a,Z_c denote the total number of anion or cation valence electrons. After some algebra, the cohesive energy can be written as a sum of three terms:

$$-E_{\text{coh}}=E_{\text{tot}}-E_{\text{atom}} =E_{\text{cov}}+E_{\text{overlap}}+E_{\text{transfer}} , \tag{2.18}$$

$$E_{\text{cov}}=\frac{1}{N}\sum_{n,\mathbf{k}}^{\text{occ}}\varepsilon_{n\mathbf{k}}-\sum_{\lambda,i}\varepsilon_{\lambda i} , \tag{2.19}$$

$$E_{\text{overlap}}=\sum_{\lambda,i}Q_{\lambda i}f_{\lambda i} , \tag{2.20}$$

$$E_{\text{transfer}}=\sum_{\lambda,i}(Q_{\lambda i}-Z_{\lambda i})w_{\lambda i} +\tfrac{1}{2}Z^{*2}(U_a+U_c-2U_M) , \tag{2.21}$$

where

$$Z^*=Z_c-Q_c=-(Z_a-Q_a) , \tag{2.22}$$

is the effective charge, and $Q_{\lambda i}$ has been defined in Eq. (2.6). The cohesive energy in Eq. (2.18) is the energy of separation of the solid into neutral atoms. Although only the sum of the three terms of E_{coh} can be well defined, the splitting in Eq. (2.18) allows a physically transparent interpretation of the cohesive properties of solids.

The covalent energy contribution E_{cov} in Eq. (2.19) represents mainly the short-range electron-ion interaction and has been defined in such a manner that it vanishes if all hopping matrix elements $t_{\lambda\lambda'}$ are zero. It is therefore a measure for the tendency of the anions and cations to equalize their electron occupancies.

The overlap energy is a repulsive contribution to E_{tot} and arises from the orthogonalization of the atomiclike orbitals. It can be predominantly ascribed to the increase of the kinetic energy of the valence electrons upon compression of the solid.[44]

The transfer energy Eq. (2.21) consists of two terms. The first term on the rhs of Eq. (2.21) takes into account the different population of the orbitals in the solid compared to neutral atoms. This energy originates both in the inter-atomic charge transfer and in promoting electrons from s to p orbitals within the atoms in the solid. The second term in Eq. (2.21) is the electrostatic energy.

So far, we have assumed the electrostatic potential V in Eqs. (2.5) and (2.11) to be strictly Coulombic. For short

distances, however, the charge overlap will render arbitrary any distinction between the intra-atomic electron-electron interaction and the inter-atomic Coulomb interaction in Eqs. (2.5) and (2.21). The simplest way to take this into account is to assume that the electrostatic terms in Eqs. (2.5) and (2.21) cancel for short distances and then to interpolate V for long and for short distances. This leads to[46]

$$V(\mathbf{R}_I-\mathbf{R}_{I'}) = \frac{e^2}{|\mathbf{R}_I-\mathbf{R}_{I'}|}\left[1-\exp\left[-\frac{(U_a+U_c)\,|\mathbf{R}_I-\mathbf{R}_{I'}|}{2e^2}\right]\right]. \tag{2.23}$$

In order to evaluate $\varepsilon_{\lambda I}$ in Eq. (2.5), this interaction has to be summed over all lattice points I. It turns out that the sum over all lattice points in Eq. (2.5) can be well approximated for cubic crystals by the analytical form

$$U_M = \frac{e^2\alpha_M}{d}\left\{1-\exp\left[-\left[\frac{U_a+U_c}{2}\right]\Big/\left[\frac{e^2\alpha_M}{d}\right]\right]\right\}. \tag{2.24}$$

This form guarantees that the term $U_a+U_c-2U_M$ is positive for all d, such that $E_{\rm tot}$ has a minimum rather than a maximum as a function of Z^* in the ionic limit ($t_{\lambda\lambda'}\to 0$).[15] We have used Eq. (2.24) throughout this paper although the difference between U_M in Eqs. (2.13) and (2.24) is small (typically less than 20%) and either form could be used. The influence of the differences between Eqs. (2.13) and (2.24) on the results is discussed in Sec. IV.

By minimizing $-E_{\rm coh}$ or, equivalently, $E_{\rm tot}$, in Eqs. (2.18)—(2.22) as a function of volume, we are now in the position to calculate static equilibrium properties, structural phase transition pressures, and phonons for the solids considered. Once the universal constants η and K have been determined, the only empirical inputs required for any given solid are the atomic-orbital energies w_s and w_p, and the intra-atomic Coulomb repulsion U (see Table I).

III. RESULTS

First, we present results for the undistorted structures. Equations (2.2), (2.5), and (2.6) were solved self-consistently with respect to the occupancies Q_I. Then the cohesive energy in Eq. (2.18) was calculated as a function of the volume for the NaCl, the CsCl, and the ZnS structure of each compound and the stable phase for zero pressure, the equilibrium volume V_0, bulk modulus B_0, derivative of B_0 with pressure, transition pressures, and corresponding volume changes were obtained. As an additional result of the self-consistency procedure, the electronic band structures are obtained for all three cubic phases.

The $\mathbf{k}$ sums were performed using up to 19 special $\mathbf{k}$ points,[47] and Eqs. (2.5) and (2.6) were iterated to give the total energies with an accuracy of better than 0.01 eV. Mostly, two special $\mathbf{k}$ points[47] and less than ten iterations are sufficient. The calculations can easily be performed on a personal computer. The calculated total energies were fit to polynomials as a function of the lattice constant and subsequently their minima and derivatives were computed.

A. Band structures

It was demonstrated previously that the overall feature of the valence and lowest conduction bands of tetrahedrally coordinated semiconductors can be well represented within empirical tight-binding models.[40,42] We find that the use of *universal* diagonal and off-diagonal matrix elements in the electron Hamiltonian according to the present model gives very satisfactory energy bands also for sixfold and eightfold coordinated semiconductors and insulators.

In Fig. 1 the band structure of GaAs in the zinc-blende ($B3$) and the rocksalt ($B1$) phases is shown. It was calculated at the predicted equilibrium volumes (cf. Fig. 3). In the $B3$ phase, the model gives the energy gap and width of the uppermost valence bands as 1.38 and 6.72 eV, in reasonable agreement with the experimental values, given by 1.52 and 6.9 eV,[48] respectively. It is remarkable that all major features of the band structure in the $B1$ phase agree excellently with *ab initio* calculations;[23] GaAs in the $B1$ phase is predicted to be metallic, also in agreement with Ref. 23.

In Fig. 2 the band structure of NaCl is depicted as a typical example for an ionic solid. The upper valence bands of NaCl exhibit all major characteristic features of rocksalt-phase crystals which were discussed previously in Ref. 49. The calculated band gap at $\mathbf{k}=\mathbf{0}$ and the anion valence-band width is 6.8 and 4.4 eV. The experimental data are 8.5 eV (Ref. 50) and 4.1±0.2 eV (Ref. 51), respectively.

These figures illustrate that the present universal tight-binding model is able to predict semiquantitatively the band structures for both covalent and ionic and both fourfold and sixfold coordinated solids. We have actually calculated the band widths and gaps at $\mathbf{k}=\mathbf{0}$ for 62 binary solids, including IV-IV, III-V, II-VI, and I-VII compounds. The agreement with experiment is generally satisfactory. The band gaps are mostly somewhat underestimated (which is not unreasonable since we use a

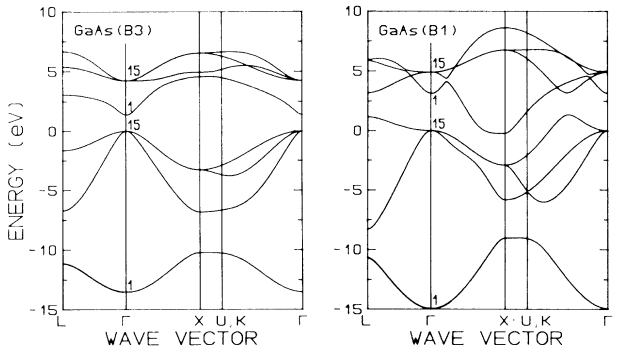

FIG. 1. Calculated band structure of GaAs (a) in the zinc-blende ($B3$) phase and (b) in the rocksalt ($B1$) phase.

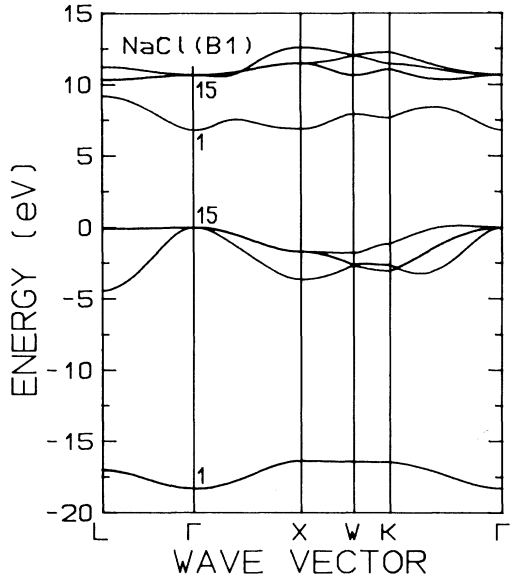

FIG. 2. Calculated band structure of NaCl in the rocksalt ($B1$) phase.

Hartree-type approximation[52]) and the predicted band widths for I-VII compounds are somewhat overestimated, typically by 30% (see Sec. IV).

B. Structural properties

In Fig. 3 the theoretical equilibrium bond lengths are compared with the experimental ones for the 62 compounds studied in this paper. Figures 4(a) and 4(b) depict the trends in the bulk moduli as a function of volume and also compare the present theoretical results with experiment. The data exhibit chemical trends which have been

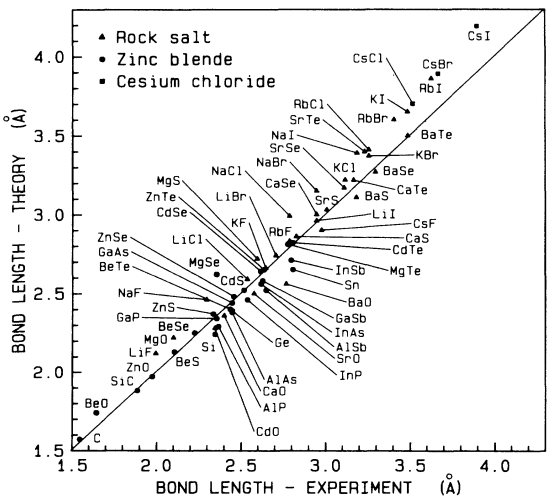

FIG. 3. Comparison of predicted bond lengths with experimental data. The experimental bond lengths for I-VII compounds are taken from Ref. 53, all other data are from Ref. 54.

studied in several papers.[3,64–66] These trends are well reproduced by our model and will be explained in Sec. V. For the group-IV, III-V, and II-VI compounds, the agreement with the data is very good, whereas the theoretical bulk moduli B_0 for the I-VII compounds depend somewhat too strongly on volume V, $B_0 \propto V^{-1.8}$ compared to $B_0 \propto V^{-1.0}$ in the data.

The derivative of the bulk modulus with respect to pressure B_0' is a c number which, qualitatively, reflects the slope of the repulsive potential between atoms in the solid. In the present model the calculations give universally $B_0' = 4.5 \pm 0.4$ irrespective of the equilibrium structure and compound, which seems to be in accord with the experimental data for group-IV, III-V (Ref. 55), II-VI (Refs. 64 and 67), and I-VII (Ref. 68) compounds. Comparison with experiment in I-VII materials is hampered by the appreciable scattering in these data. In NaCl, for example, the theory gives $B_0' = 4.75$, whereas published data vary from 4.0 to 6.0.[68]

C. Relative stability of phases and structural phase transitions

We have performed calculations for compounds in NaCl ($B1$), CsCl ($B2$), and ZnS ($B3$) phases and calculated the total energy in each phase as a function of volume. Since the group-IV and III-V compounds become metallic in the high-pressure phase and tend to transform to noncubic phases, we focused on II-VI and I-VII crystals.

A phase transformation as a function of pressure can be calculated by equating the Gibbs free energies G_A, G_B of the two phases A and B. For given pressure, we minimized $G = E_{\text{tot}} + PV$ as a function of V for each phase and calculated $\Delta G = G_A - G_B$. By varying the pressure, we determined the zero of ΔG, which occurs at $P = P_t$ and at volumes equal to the transition volumes V_t^A and V_t^B for phases A and B, respectively. P_t at zero temperature is then given by

$$P_t = \frac{E_{\text{tot}}(V_t^A) - E_{\text{tot}}(V_t^B)}{V_t^A - V_t^B} . \tag{3.1}$$

Figures 5(a) and 5(b) show the equations of state for ZnS and CaO for the three cubic phases. Among these structures, the lowest phase in energy is predicted to be $B3$ for ZnS and $B1$ for CaO, in agreement with experiment. We point out that the minima of the total energies as a function of volume occur in the same order $B2$, $B1$, and $B3$ in both cases. In fact, this is a universal feature of all compounds investigated in this paper, as will be explained physically in Sec. V C, and it is in accord with experiment: As a function of pressure, only transitions from zinc-blende to rocksalt and rocksalt to cesium chloride have been observed, whereas no pressure-induced transitions from rocksalt to zinc-blende or cesium chloride to rocksalt are known.[69]

Figure 6 summarizes the predictions for transition pressures for II-VI compounds together with the known experimental data. The chemical trends in the theoretical results are in good agreement with the available data and are insensitive to details of the model. In particular, the

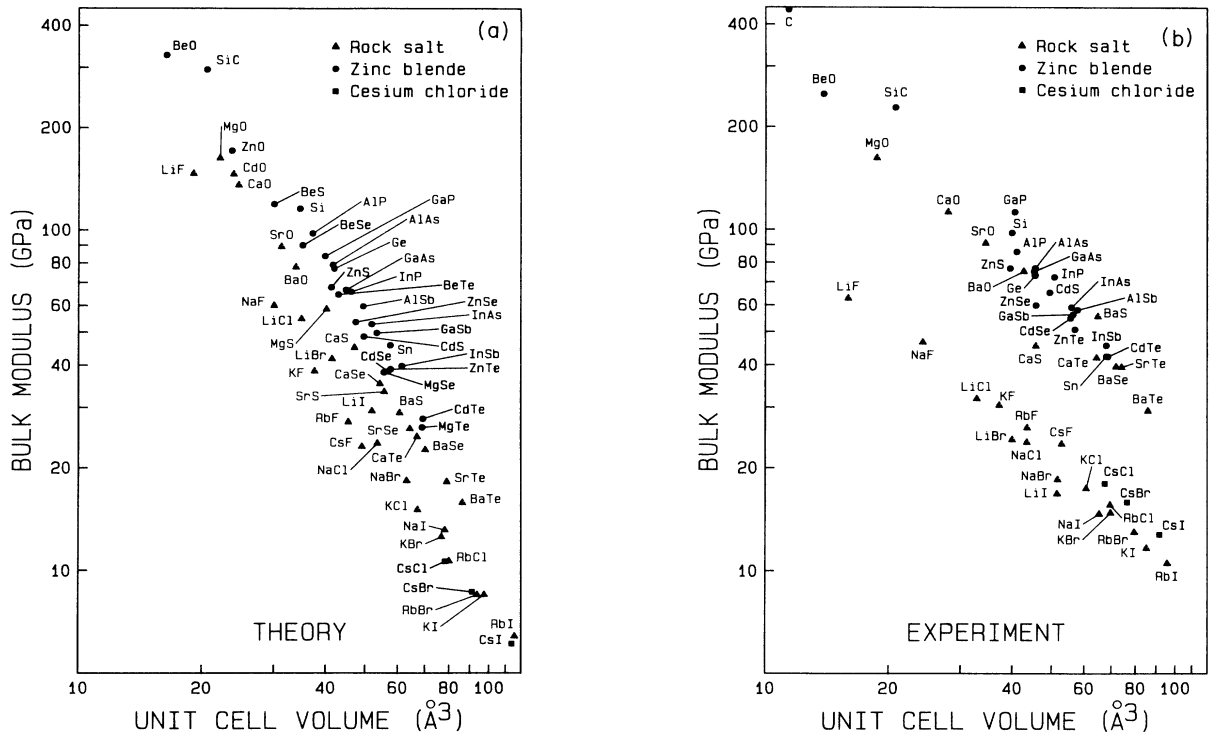

FIG. 4. (a) Predicted bulk modulus for cubic, binary compounds plotted as a function of the calculated equilibrium volume. (b) Experimental bulk modulus vs experimental equilibrium volumes (the latter are from Refs. 53 and 54). The data are from Refs. 55 and 56 (group IV and III-V's), Ref. 57 (zinc and cadmium chalocogenides), Ref. 58 (BeO), Ref. 59 (MgO), Ref. 60 (CaO, SrO, BaO), Ref. 61 (BaS), Ref. 62 (BaSe, BaTe), Ref. 63 (CaS), Ref. 64 (CaTe, SrTe), and Ref. 6 (I-VII's).

theory reproduces the puzzling strong cation dependence (e.g., CaTe, SrTe, BaTe) and the relative anion independence (e.g., ZnO, ZnS, ZnSe, ZnTe) of the observed transition pressures. The physical reason for this effect was not understood so far,[69] but can be easily explained in terms of the present model (see Sec. V).

Some detailed theoretical results and the experimental data for crystal properties associated with structural phase transformations as a function of hydrostatic pressure are summarized in Tables II—V. Previous theoretical results are also included in Tables II and III. For all II-VI compounds except two (namely MgS and CaTe) the present

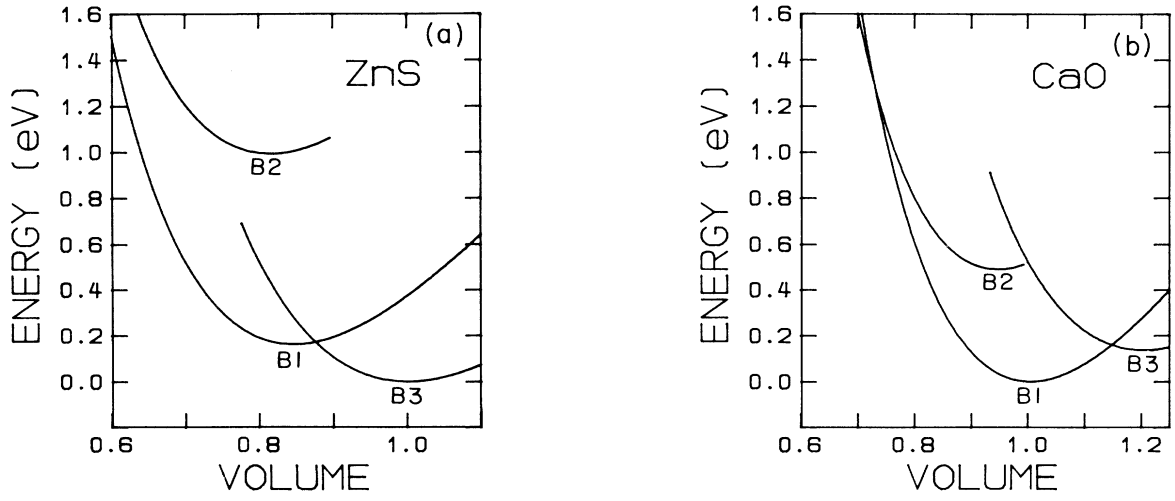

FIG. 5. Calculated total energy per unit cell as a function of volume (relative to equilibrium volume) for the rocksalt ($B1$), the cesium chloride ($B2$) and the zinc-blende ($B3$) phase of (a) ZnS and (b) CaO.

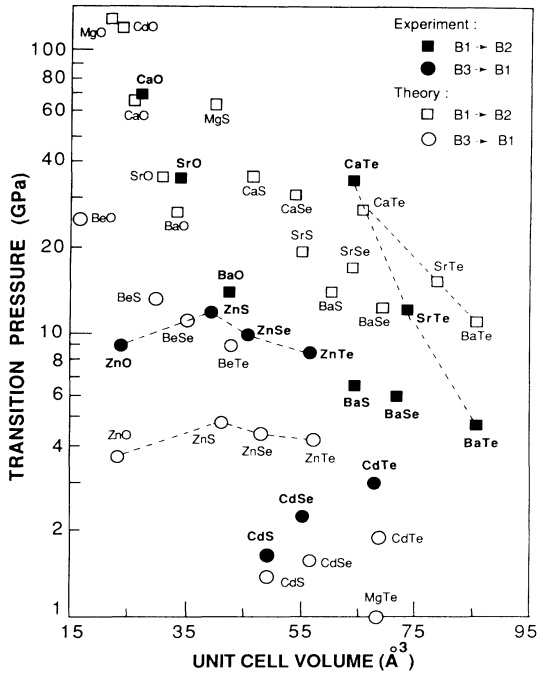

FIG. 6. Theoretical and experimental transition pressures for the indicated structural phase transitions vs the calculated and experimental equilibrium volume at zero pressure, respectively. The dashed lines indicate the chemical trends in the transition pressures and are shown only to guide the eye. The transition pressures depend strongly on the cation, but only weakly on the anion. The sources of the experimental data are cited in the captions of Tables II and III.

model gives the phase lowest in energy at zero pressure in agreement with the data.[55] We have not, however, discriminated between the wurzite and the zinc-blende phase in the calculations.

Tables II and III show that the chemical trends in the cohesive energies are also correctly reproduced by the model. Quantitatively, the cohesive energies are somewhat overestimated, particularly for oxides which have very small bond lengths.

In Tables IV and V the theoretical results for the structural energy differences between the cubic phases of I-VII compounds are listed. In all cases, the minimum of the total energy in the $B3$ phase is correctly obtained to be energetically higher than the total energy in the $B1$ phase. We find this difference to be significantly larger for the I-VII compounds than for the II-VI compounds, in accord with intuitive ionicity arguments.[3] The energy of the minimum of the $B2$ phase, however, is found to be systematically lower than the $B1$ phase, which disagrees with experiment. All I-VII compounds except CsCl, CsBr, CsI actually crystallize in the $B1$ phase. We shall discuss the origin of these results in Sec. IV.

D. Transverse optical phonons

As an example for dynamic properties of solids, we have calculated long-wavelength transverse-optical (TO) phonons in different crystal structures. In the adiabatic approximation and for binary crystals, this amounts to the calculation of the total energy of the crystal as a function of the displacement u of the two sublattices relative to each other.

To third order in u, the change of the total energy with u can be written as

$$\Delta E_{\rm tot}(u)=2\pi^2 M\nu_{\rm TO}^2 u^2+k_{xyz}\left[\frac{u}{\sqrt{3}}\right]^3, \tag{3.2}$$

where M is the reduced cell mass, $\nu_{\rm TO}$ is the harmonic TO-phonon frequency, and k_{xyz} denotes the cubic anharmonic force constant.[91] The latter is nonzero only in the absence of inversion symmetry ($B3$ phase).

The displacement u changes the off-diagonal elements of the one-electron Hamiltonian H in Eq. (2.2) in $\mathbf{k}$ space via the d dependence of $t_{\lambda\lambda'}$, the direction cosines and the phase factors $\exp(i\mathbf{k}\cdot\mathbf{R})$. The k sums in Eqs. (2.6) and (2.19) were performed using 17 special $\mathbf{k}$ points in the $B1$ phase and 5 in the $B3$ phase to obtain convergent results. This corresponds to six and two special $\mathbf{k}$ points, respectively, in the undistorted crystal.[47]

The long-range interatomic interaction terms in Eqs. (2.5) and (2.11) are obtained by summing the potential $V(\mathbf{R}_I-\mathbf{R}_{I'})$ over all lattice sites, where $\mathbf{R}_I$ denote the displaced lattice vectors. We find that the numerically performed summation can be very well approximated by the following analytical form:

$$\sum_{I\neq 0}(Z_I-Q_I)V(\mathbf{R}_I)=(Z_c-Q_c)\tilde{U}_M\left[1-\exp\left[-\frac{U_a+U_c}{2\tilde{U}_M}\right]\right], \tag{3.3}$$

where we have chosen the origin at the cation site and $\tilde{U}_M$ denotes the Madelung energy, analogous to Eq. (2.13), for the displaced lattice. To second order in u, $\tilde{U}_M$ in Eq. (3.3) can be evaluated analytically for the $B1$, $B2$, and $B3$ phase,[92]

$$\tilde{U}_M=\frac{e^2\alpha_M}{d}+\frac{e^2 4\pi}{3\Omega_0}u^2, \tag{3.4}$$

where Ω_0 is the unit cell volume. We calculated $\nu_{\rm TO}$ as a function of pressure in the $B1$, $B2$, and the $B3$ phase. The most striking result is that this model predicts a strong TO-phonon softening, i.e., a reduction of $\nu_{\rm TO}$ by an order of magnitude, across a pressure-induced phase transformation from the $B3$ to the $B1$ phase for II-VI compounds. We find a strong TO-phonon softening for all tetrahedral II-VI compounds and summarize the results in Table VI. These materials probably do not become metallic for pressures near the transition pressure.[80,93] The physical origin of this effect is analogous to the phonon-instability in ferroelectrics and will be discussed in Sec. V. To our knowledge no experimental data for $\nu_{\rm TO}$ across the $B3$-$B1$ transformation are published. Yet a TO softening across the $B3$-$B1$ phase transition for metallic GaAs,[23] and a softening of $\nu_{\rm LO}$ ($\mathbf{q}=\mathbf{0}$) and of zero-boundary phonons in metallic high-pressure phases of Si was predicted recently.[24]

TABLE II. Predicted transition pressure P_t, transition volume V_t relative to the zero pressure volume V_0, and relative volume change from the zinc-blende ($B3$) to the rocksalt ($B1$) transition of II-VI compounds. $E_{\min}$ denotes the minimum of the total energy in each labeled phase and E_{coh} is the cohesive energy. The observed stable phase of all compounds is the zinc-blende (or wurzite) structure. The experimental data are given in parentheses, and previous theoretical results are given below the results of this paper.

Compound	P_t ($B3\rightarrow B1$) (GPa)	V_t^{B3}/V_0^{B3}	$1-V_t^{B1}/V_t^{B3}$	$E_{\min}^{B1}-E_{\min}^{B3}$ (eV)	$E_{\min}^{B2}-E_{\min}^{B3}$ (eV)	E_{coh} ($B3$) (eV)
BeO	25.1	0.94	0.14	0.32	1.85	26.7 (12.2[a])
ZnO	3.6 (9.0[b])	0.98	0.16	0.07	1.01	21.9 (7.6[a])
BeS	13.2	0.91	0.14	0.32	1.54	14.9 (8.6[a])
ZnS	4.7 (11.7-18[b–d])	0.94	0.15	0.16	0.99	12.5 (6.4[a])
	20–30[e]	0.93[e]	0.16–0.2[e]			
CdS	1.4 (1.65–2.5[f–j])	0.97 (0.9[g])	0.16 (0.2[h])	0.06	0.67	11.4 (5.7[a])
BeSe	11.2	0.91	0.14	0.32	1.47	12.4
MgSe	0.7	0.98	0.16	0.03	0.58	9.3
ZnSe	4.4 (10–14[b–d,k])	0.93	0.15	0.17	0.98	10.7 (5.2[a])
	15–23,[e] 28.2[l]	0.93,[e] 0.80[l]	0.16–0.2,[e] 0.21[l]			
CdSe	1.6 (2.3–3[g,h])	0.96 (0.91[g])	0.15 (0.2[h])	0.08	0.67	9.7 (4.8[a])
BeTe	9.1	0.90	0.14	0.33	1.42	10.2
MgTe	1.0	0.97	0.15	0.06	0.60	7.3 (5.7[a])
ZnTe	4.2 (8.5–12[b,c,m])	0.92	0.14	0.21	1.01	8.7 (4.6[a])
	10–15,[e] 18.8[n]	0.92[e]	0.17–0.2,[e] 0.08[n]			
CdTe	1.9 (3–4[f,g,o,p])	0.94 (0.93,[o] 0.09[p])	0.15 (0.17,[o] 0.16[p])	0.11	0.71	7.9 (4.1[a])
	1.5–5.6,[e] 7.2[n]	0.92[e]	0.17–0.2,[e] 0.16[n]			

[a]Reference 70.
[b]Reference 69.
[c]Reference 71.
[d]Reference 72.
[e]Reference 73.
[f]Reference 74.
[g]Reference 75.
[h]Reference 76.
[i]Reference 77.
[j]Reference 78.
[k]Reference 79.
[l]Reference 80.
[m]Reference 81.
[n]Reference 82.
[o]Reference 83.
[p]Reference 84.

In Table VII, our calculations of ν_{TO} and related properties for zero pressure are given for a few typical materials and compared to published experimental and previous theoretical *ab initio* results. It is noticable that the present simple model is able to predict even subtle nonlinear dynamical properties such as the anharmonic force constants in reasonable agreement with experiment or first-principles calculations.

We have actually computed ν_{TO} for all compounds considered in the previous section. It seems sufficient to say here that the results are generally satisfactory. The model tends to underestimate ν_{TO} somewhat for materials in the $B1$ phase, particularly for the oxides where the bond length is exceptionally small. For CaO, for example, we obtain $\nu_{\text{TO}}=3.6$ THz compared to the experimental value of 8.7 THz.[55]

IV. CHOICE OF PARAMETERS

Since the aim of this paper is to show that a simple and universal model is able to provide both the essential qualitative physics and semiquantitative results for solid-state properties in a wide range of materials, we attempted to use as few empirical parameters as possible. In Table VIII we exemplify the effects of changing particular parameters or assumptions in this model. One can see that this theory is quite insensitive to modifications, provided the parameters reflect the chemical trends in the atomic data.

We used one s and three p states per atom throughout. Actually, this is somewhat artificial for I-VII compounds such as NaCl, since the Na-p state contributes very little to cohesion. In this case the Na-p basis state plays the role of a peripheral state which simulates both more distant than nearest-neighbor interactions as well as higher excited states. Similar arguments apply to Sr and Ba compounds, where the conduction bands are actually d-like but are simulated by p states in our model.

The inclusion of a peripheral s state, as was done previously in Ref. 42, affects only details of the conduction bands and influences the total energy only negligibly. Therefore s^* states were neglected. In addition, in Ref. 42 the diagonal Hamiltonian matrix elements $\varepsilon_{\lambda I}$ for semiconductors were obtained by scaling the atomic orbital energies $w_{\lambda I}$ by factors of 0.6 for p states and 0.8 for s states. This is consistent with the present model: We have constructed the solid-state corrections to $w_{\lambda I}$ explicitly [see Eq. (2.5)] and included some second-neighbor matrix elements. The resulting effective $\varepsilon_{\lambda I}$ are indeed close to the ones determined previously,[42] apart from an irrelevant overall shift.

The transfer or offsite matrix elements $t_{\lambda\lambda'}$ were taken from Ref. 42 for nearest neighbors, although Harrison's parameters could have been used as well.[15] The important point is that we implicitly use the assumption that the parameters $\eta_{ll'm}$ are independent of the structure. This is

TABLE III. Predicted transition pressure P_t, transition volume V_t relative to the zero pressure volume V_0, and relative volume change from the rocksalt ($B1$) to the cesium chloride ($B2$) transition of II-VI compounds. $E_{\min}$ denotes the minimum of the total energy in each labeled phase and $E_{\rm coh}$ is the cohesive energy. The observed stable phase of all compounds is the rocksalt structure. The experimental data are given in parenthesis, and previous theoretical results are given below the results of this paper.

Compound	P_t ($B1\rightarrow B2$) (GPa)	V_t^{B1}/V_0^{B1}	$1-V_t^{B2}/V_t^{B1}$	$E_{\min}^{B2}-E_{\min}^{B1}$ (eV)	$E_{\min}^{B3}-E_{\min}^{B1}$ (eV)	$E_{\rm coh}$ ($B1$) (eV)
MgO	126	0.70	0.05	0.68	0.07	20.7 (11.6[a])
	172–1050[b–f]	0.38–0.68[b,c,e,f]	0.04–0.11[b,c,e,f]	0.73–2.04[b–e,g,h]	0.06[g]	10.0–11.6[b,c,g]
CaO	66.8 (70±10[h])	0.75 (0.74[i])	0.05 (0.11[i])	0.49	0.14	20.0 (11.0[a])
	106–162,[d,e] 55[f]	0.69,[e] 0.75[f]	0.07–0.08[e,f]	1.21–1.43[d,h,e]	0.30[g]	
SrO	35.6 (36±4[j])	0.79 (0.80[j])	0.06 (0.12[j])	0.36	0.18	18.8 (10.4[a])
	88–95,[e] 36[f]	0.65–0.78[e,f]	0.06–0.08[e,f]	1.18–1.22[e]		
BaO	26.9 (14±0.5[k])	0.80	0.06	0.31	0.19	18.7 (10.2[a])
	88–95,[e] 21[f]	0.62–0.67,[e] 0.82[f]	0.05,[e] 0.08[f]	1.15–1.19[e]		
CdO	118.3	0.70	0.05	0.67	0.04	20.3 (6.4[a])
MgS	64.0	0.65	0.05	0.57	−0.01	11.1 (8.0[a])
CaS	35.5	0.70	0.05	0.42	0.04	11.1 (9.7[a])
				−0.07[g]		10.1[f]
SrS	19.3	0.74	0.05	0.31	0.09	10.4 (9.3[a])
BaS	14.0 (6.5[l])	0.76 (0.90[l])	0.05 (0.14[l])	0.27	0.10	10.4 (9.3[a])
CaSe	31.1	0.68	0.05	0.42	0.02	9.3 (7.8[a])
SrSe	17.2	0.72	0.05	0.32	0.06	8.8
BaSe	12.6 (6.0±2[m])	0.75	0.06 (0.14[m])	0.27	0.08	8.8 (10.3[a])
	5.6[n]	0.90[n]	0.15[n]	0.31[n]		
CaTe	27.5 (35±5[o])	0.65 (0.70[o])	0.05 (0.11[o])	0.42	−0.01	7.4
SrTe	15.4 (12±1[o])	0.69 (0.83[o])	0.05 (0.11[o])	0.32	0.03	6.9
BaTe	11.2 (4.8±0.3[p])	0.72	0.05 (0.13[p])	0.28	0.05	7.0
	3.2[n]	0.93[n]	0.14[n]	0.20[n]		

[a]Reference 70.
[b]Reference 21.
[c]Reference 27.
[d]Reference 34.
[e]Reference 7.
[f]Reference 35.
[g]Reference 85.
[h]Reference 33.
[i]Reference 86.
[j]Reference 87.
[k]Reference 88.
[l]Reference 67.
[m]Reference 89.
[n]Reference 26.
[o]Reference 64.
[p]Reference 90.

strongly supported by the present results for the electronic band structures, Figs. 1 and 2. In addition, the nearest-neighbor distances vary by more than a factor of 2 in the materials studied in this paper, which provides a stringent and successful test for the d^{-2} dependence of $t_{\lambda\lambda'}$ in Eq. (2.4). The next-nearest neighbors have little influence on the cohesive properties as can be deduced from Table VIII. However, the energy gaps at $\mathbf{k}=0$ are overestimated by typically 3 eV if the next-nearest neighbor couplings are neglected. We therefore fitted $\eta_{sscs\sigma}$ and $\eta_{papa\sigma}$ to obtain energy gaps in semiconductors in approximate overall agreement with the experimental band gaps.

The next-nearest-neighbor couplings have the additional effect of raising the top of the valence band at $\mathbf{k}=0$ with respect to the $\mathbf{k}$ points at the boundary of the Brillouin zone and therefore favor direct gaps. For sake of universality, the scaling of these matrix elements with bond length was taken to be d^{-2} as well.[49]

The d dependence of the overlap matrix elements S was chosen empirically as d^{-3} universally. A weaker d

TABLE IV. Predicted total energy difference per unit cell (in meV) between the minimum of the zinc-blende ($B3$) and the rocksalt ($B1$) phases of I-VII compounds.

	F	Cl	Br	I
Li	546	352	310	258
Na	475	320	284	242
K	417	284	269	220
Rb	365	253	230	190
Cs	343	235	216	190

TABLE V. Predicted total energy difference per unit cell (in meV) between the minimum of the cesium chloride ($B2$) and the rocksalt ($B1$) phases of I-VII compounds.

	F	Cl	Br	I
Li	−112	−42	−27	2
Na	−209	−122	−98	−69
K	−217	−133	−104	−88
Rb	−193	−126	−107	−87
Cs	−183	−119	−102	−84

TABLE VI. Predicted long-wavelength transverse-optical-phonon frequencies at the $B3 \rightarrow B1$ transition pressure.

Compound	ν_{TO} ($\mathbf{q}=0, B3$) (THz)	ν_{TO} ($\mathbf{q}=0, B1$) (THz)
ZnO	18.8	1.8
ZnS	11.0	1.2
ZnSe	8.4	1.0
ZnTe	7.1	0.9
CdS	8.3	0.8
CdSe	5.7	0.4
CdTe	4.6	0.5

dependence, e.g., $S \propto d^{-2}$, underestimates the bulk moduli and the optical-phonon frequencies by approximately a factor of 3 in ionic compounds, whereas a stronger dependence, e.g., $S \propto d^{-4}$, overestimates these quantities in semiconductors and stabilizes the $B1$ phase relative to the $B3$ phase in II-VI compounds.

In the $B2$ phase, the next-nearest neighbors are closer to the nearest neighbors than in the $B1$ or $B3$ phase. In the present model, we assumed the d dependence of the overlap to be the same for nearest and next-nearest neighbors. The static cohesive properties, such as the bulk modulus and bond lengths, as well as the relative stability of the $B3$ and $B1$ phase are quite insensitive to this assumption. However, the relative stability of the $B1$ and $B2$ phase can be affected by modifications of this assumption. In particular, the model developed in Sec. II stabilizes most of the I-VII compounds in the $B2$ rather than in the $B1$ phase (Table V). We can obtain the correct ordering of structures for I-VII compounds by assuming a stronger d dependence of the next-nearest-neighbor contribution to the overlap interaction. Using a functional form for S analogous to Eq. (2.8) but using $S \propto d^{-6}$ for second-nearest neighbors, we obtain transition pressures for all I-VII compounds in excellent agreement with experiment.

V. UNDERSTANDING THE CHEMICAL TRENDS

Many empirical models for ionic crystals[2,6,7,8] invoke the classical point charge picture. In such a model, the cohesive properties result from a balance between the Madelung energy and an overall repulsive force, which makes it difficult to discuss chemical trends. It is widely believed that this ionic picture is supported by the calculated or measured charge density of ionic crystals, which indeed suggests closed-shell ions. We should like to point out, however, that the static charge density is very insensitive to charge transfer or the degree of ionicity. As an illustrative example, one may calculate the approximate electronic valence charge density of NaF either by superimposing Hartree-Fock charge densities of free Na^{+1} and F^{-1} ions or, alternatively, by superimposing neutral-atom charge densities of Na^0 and F^0.[43] One finds that these two types of charge densities are practically indiscriminable and differ by less than 5% outside of the core regimes. One may even calculate x-ray integrated intensities for NaF, using either neutral-atomic or ionic form factors. Again, the results are sufficiently similar that the experimental data cannot discriminate between them.[98,99] In covalent solids, Harrison[100] pointed out several years ago that the valence charge density of aluminum, calculated in the zinc-blende phase, is practically identical to that of silicon, even though such a crystal is a metal and unstable.

In this section, we show that the present model gives new qualitative insight into the physical mechanisms governing the trends in the structural properties of nonmetallic solids. The understanding of the physical mechanisms is greatly facilitated by first discussing the trends in the individual contributions to the total energy which are given in Eqs. (2.18)—(2.22). Although such a breakup is not unique, it provides a very useful framework for interpreting the results.

The overlap energy is a repulsive contribution to E_{tot} and the calculations show that it scales approximately as d^{-5}, where d is the nearest-neighbor distance. In a series of compounds AB, the overlap energy becomes more

TABLE VII. Predicted long-wavelength transverse-optical-phonon frequencies, their pressure derivatives at zero pressure, and the associated cubic anharmonic force constants. The experimental data are given in parentheses, and previous theoretical results are given below the results of this paper.

Compound	ν_{TO} ($\mathbf{q}=0$) (THz)	$d\nu_{TO}/dp$ (THz GPa^{-1})	$d^2\nu_{TO}/dp^2$ (THz GPa^{-2})	k_{xyz} (eV/Å^3)
Si	18.6 (15.6[a])	0.19 (0.16[a])	−0.005(−0.004[b])	−47.5 (−35.1[c,d])
	15.2,[c] 15.0[d,e]			−32.8,[c] −34.8,[d] −47.5[e]
GaAs	9.0 (8.2[a])	0.17 (0.13[a])	−0.010 (−0.006[f])	−26.7
	8.29[g]			−35.2[g]
ZnSe	7.2 (6.1[a])	0.20 (0.16[a])	−0.010	−19.6
NaCl	3.3 (4.9[a])	0.47 (0.46[a])	−0.126	0
	4.9[h]			

[a]Reference 57.
[b]Reference 94.
[c]Reference 22.
[d]Reference 95.
[e]Reference 91.
[f]Reference 96.
[g]Reference 97.
[h]Reference 20.

TABLE VIII. Summary of changes of the results for CaO with changes in the parameters. The entries are lattice constant, bulk modulus at zero pressure, cohesive energy, transition pressure, total energy differences, and the electronic energy gap at $\mathbf{k}=\mathbf{0}$.

Change of parameters	a_0 ($B1$) (Å)	B_0 (GPa)	$E_{\rm coh}$ ($B1$) (eV)	P_t ($B1\rightarrow B2$) (GPa)	$E_{\rm min}^{B2}-E_{\rm min}^{B1}$ (eV)	$E_{\rm min}^{B3}-E_{\rm min}^{B1}$ (eV)	$E_{\rm gap}$ (eV)
none	4.72	120.4	20.0	66.8	0.49	0.14	7.95
a	4.34	183.3	23.2	138.1	0.67	0.08	10.02
b	4.67	123.4	16.8	96.5	0.62	0.08	6.34
c	4.54	151.2	23.0	120.4	0.66	0.05	9.20
d	4.33	135.6	18.4	40.4	0.33	0.16	5.96
e	4.81	97.5	21.2	26.4	0.23	0.27	8.71
f	4.70	123.4	20.3	81.3	0.58	0.19	11.19
g	4.60	170.3	24.7	82.1	0.76	0.19	14.29

[a]Increase of constant K by 25%.
[b]Decrease of atomic-orbital energy w_{sc} by 2.5 eV.
[c]Decrease of atomic energy w_{pc} by 2.5 eV.
[d]Decrease of all offsite matrix elements $t_{\lambda\lambda'}$ by 25%.
[e]Decrease of all Coulomb repulsions U_a, U_c by 25%. The constant r_0 in Eq. (2.9) is not changed.
[f]All second-nearest-neighbor matrix elements $t_{\lambda\lambda'}$ are set equal to zero.
[g]Strictly Coulombic long-range electron-ion and electron-electron interaction. Equation (2.13) is used instead of Eq. (2.24).

repulsive when either A or B vary downward in a given valence column of the Periodic Table. This follows from the explicit form of the overlap matrix [see Eq. (2.8) and Table I] and is also physically plausible due to the increasing size of the heavier atoms.

The covalent energy contribution Eq. (2.19) to $E_{\rm tot}$ is an effectively attractive energy and is also inversely proportional to d. Qualitatively, the covalent energy contribution becomes more attractive when the difference between the anion and cation orbital energies decreases. This can be explicitly seen in the limiting case of a two-state model (see Appendix) where the covalent energy is proportional to $-t^2/(w_c-w_a)$.

The charge transfer energy Eq. (2.21) depends weakly on d. It consists of two parts. The first part takes into account the different populations of the orbitals in the solid compared to neutral atoms, whereas the second part is proportional to the Madelung energy.

Figure 7 depicts the individual contributions to the total energy for a typical insulator (CaO) and a typical semiconductor (GaAs). The important point in this figure is that both the short-range overlap and the short-range covalent energy depend much more strongly on the interatomic distance than the charge transfer energy and therefore determine the chemical trends in structural properties such as lattice constant, bulk modulus, or relative phase stabilities. Only the absolute value of the cohesive energy itself is largely governed by the Madelung energy in I-VII and II-VI compounds since the overlap and the covalent energy tend to cancel each other near the equilibrium volume.

Consequently, all major static and dynamic structural properties of fourfold as well as sixfold coordinated crystals are governed by the short-range energy contributions, whereas the long-range electrostatic interaction plays only a minor role even in crystals such as NaCl. This finding is in contrast to the point-charge-type models[2,6–8] but is consistent with the experimental fact that the bandwidth of the upper valence bands is comparable in magnitude in III-V and in I-VII compounds (see Figs. 1 and 2).[101] As a consequence, the short-range electron-ion interaction is of the same order of magnitude in III-V compounds as in I-VII or II-VI materials.

In the present model the chemical trends in the structural properties of solids are determined by the orbital energies $w_{\lambda I}$ and the Coulomb repulsion energies U_I of the constituent neutral atoms which completely characterize a compound. This is in accord with the empirical concepts of electronegativity and atomic size:[5,6] For hetero-

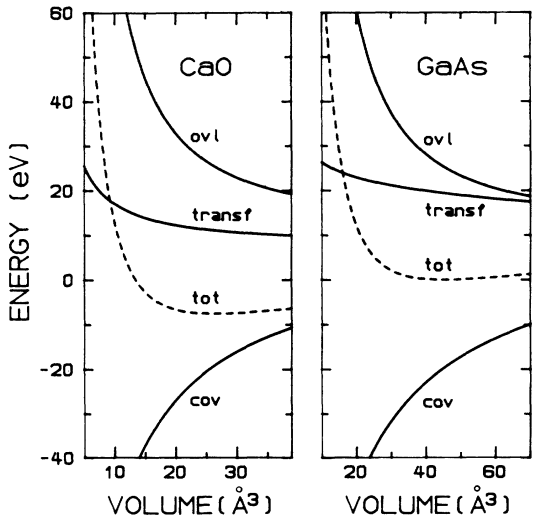

FIG. 7. The individual contributions to the calculated total energy of CaO and GaAs as a function of volume. The total energy (tot) is given by the sum of the covalent (cov), the overlap (ovl) and the charge-transfer (transf) energy. The common zero of energy is the minimum of the total energy of GaAs.

planar crystals, the difference between the cation s and anion p atomic-orbital energy provides an "atomic" electronegativity scale which generally agrees with the scale introduced by Pauling[1] and Phillips.[5] Since, in addition, the atomic-orbital energies are inversely proportional to the corresponding atomic radius, the atomic size is also incorporated.

A. Trends in bond lengths

Let us consider a sequence of compounds AB with one type of atoms fixed and the other varying downward in a given column of the Periodic Table. Examples are BeO, MgO, CaO, SrO, BaO, or alternatively, CaO, CaS, CaSe, CaTe. Since the orbitals become more extended, the repulsive overlap interaction strongly increases and consequently the equilibrium position of the total energy shifts towards larger volume in any such sequences of compounds. This explains the trends in the data shown in Fig. 3.

The attractive covalent energy supports this trend when the compounds have a common anion (e.g., oxides). In this case the cation s and anion p atomic-orbital energy differences increase with the atomic number Z of the cation (Be to Ba; see Table I) which causes the covalent energy to become less attractive. When compounds with the same cation are compared, on the other hand, the covalent energy becomes more attractive with increasing Z of the anion (O to Te; see Table I) and counteracts the trend governed by the overlap energy. We find, however, that the overlap interaction always dominates the chemical trends in the bond lengths.

B. Trends in bulk modulus

Qualitatively, the total energy may be written as

$$E_{\text{tot}}=\alpha V^{-r}-\beta V^{-s}\ , \tag{5.1}$$

the first term being proportional to the repulsive overlap energy and the second term to the attractive covalent energy. Taking the second derivative of Eq. (5.1) at the equilibrium volume $V_0=(r\alpha/s\beta)^{r-s}$, one obtains the bulk modulus

$$B_0\propto\beta V_0^{-(s+1)}\ . \tag{5.2}$$

This shows that the bulk modulus systematically decreases with increasing equilibrium volume. Numerically, we find s to be of the order of $\frac{2}{3}$. As a consequence, we find $B\propto V^{-1.6}$ in comparison to the experimental values $B\propto V^{-1.4}$ to $V^{-1.0}$. For given equilibrium volume, the trends in B are seen from Eq. (5.2) to be determined by the covalent interaction beta. As a consequence, B is predicted to decrease in a sequence of compounds with similar equilibrium bond length but decreasing β, such as Si, AlP, NaCl. As can be seen from Fig. 4, this finding explains the trends in the experimental data.

C. Trends in structural stabilities

It was noted in Sec. III C that the present model gives the equilibrium volume V_0 always in the order $B2,B1,B3$ [see Figs. 5(a) and 5(b)]. V_0 is mainly determined by that term in the total energy which depends most strongly on volume, and this is the overlap energy. For given unit cell volume, the nearest neighbor distance d is smallest in the $B3$ phase and largest in the $B2$ phase. The ratio of bond lengths is 1:1.15:1.26 for the $B3$, $B1$, $B2$ phase, respectively. The overlap energy for a unit cell of fixed volume is therefore most strongly repulsive in the $B3$ phase and least repulsive in the $B2$ phase ($E_{\text{overlap}}\propto d^{-5}$). Consequently, the minimum energy of the $B3$ phase occurs at a larger volume than the equilibrium energies of the other phases and one has $V_0^{B2}<V_0^{B1}<V_0^{B3}$.

This theory therefore predicts a *universal* sequence of structural phase transformations among the cubic phases of a given compound. As a function of pressure, structural phase transformations can occur only in the sequence zinc blende→rocksalt→cesium chloride but not in the reverse order. This result is independent of the relative total energies of these phases at their equilibrium volumes. If, for example, the rocksalt phase has the lowest equilibrium energy, such a crystal can only transform to the cesium chloride but not to the zinc-blende phases as a function of pressure [cf. Fig. 5(b)]. Actually, of course, any crystal will become metallic at sufficiently high pressure and transform to other structures, which are not considered here.

Which mechanisms determine the chemical trends in the relative stability of phases in a series of compounds? For a given unit cell volume, the covalent energy is most strongly attractive in the zinc-blende ($B3$) phase. Thus, the covalent energy favors energetically the $B3$ phase, whereas the repulsive overlap interaction always favors the $B2$ phase and, to a lesser extent, the $B1$ phase. If the difference in the cation s and anion p orbital energy decreases in a series of heteropolar compounds, the covalent energy becomes more attractive and the $B3$ phase becomes more favorable [in the simple model given in the Appendix, one has $E_{\text{cov}}\propto -t^2/(w_c-w_a)$]. This is the case in any series of compounds, where the anions vary downward in a given column of the Periodic Table. Examples are MgO ($B1$), MgS ($B1$), MgSe ($B3$), and MgTe ($B3$), where we have indicated the stable phase in parentheses. On the other hand, the overlap energy becomes dominant and the $B2$ phase more favorable if the difference in the cation s and anion p orbital energy increases in a series of compounds, such as in NaCl ($B1$), KCl ($B1$), RbCl ($B1$), CsCl ($B2$). In this case, the cations vary downward in a column.

D. Trends in transition pressures

Let us specifically consider the pressure-induced transition from the $B1$ to the $B2$ phase. The arguments given below can be immediately transferred to the transition from the $B3$ to the $B1$ phase. For a qualitative discussion, Eq. (3.1) for the transition pressure can be approximated by

$$P_t=\frac{E_{\text{tot}}^{B2}(V_0^{B2})-E_{\text{tot}}^{B1}(V_0^{B1})}{V_0^{B1}-V_0^{B2}}\ , \tag{5.3}$$

where the transition volumes have been replaced by the corresponding equilibrium volumes.[2] The trends in P_t

therefore arise from two factors: (i) the equilibrium unit cell volumes in the denominator of Eq. (5.3) and (ii) the difference in total energies in the numerator of Eq. (5.3). Since both theory and the experimental data give $V_0^{B2}-V_0^{B1}\propto V_0^{B1}$ for all compounds (see Table III), the denominator of Eq. (5.3) causes the transition pressures to decrease with increasing equilibrium volume.

The numerator of Eq. (5.3) decreases in any series of heteropolar compounds with increasing equilibrium volume, where the difference in cation s and anion p orbital energies increases. This can be understood as follows. The covalent energy is more attractive in the $B1$ phase than in the $B2$ phase, as we explained in the previous section. If $w_{s,\text{ cation}}-w_{p,\text{ anion}}$ increases, the covalent energy becomes relatively less attractive in the $B1$ phase and diminishes the numerator in Eq. (5.3). This trend supports and enhances the effect of the denominator in Eq. (5.3) for a series of compounds with the same anion (MgO, . . . , BaO). In a series of compounds with the same cation (BaS, BaSe, BaTe, or CdS, CdSe, CdTe), however, the chemical trend in the numerator counteracts the trend in the denumerator. This explains the empirically observed strong cation dependence and relative anion independence of the transition pressures of II-VI and I-VII compounds.[69] In the light of these results it is not surprising that an attempt to correlate the transition pressures with a phenomenological ionicity scale[3,14] is successful for cation-related trends but fails completely to predict the weaker trend with anions.[14]

E. Trends in optical phonons

The present model predicts a striking softening of ν_{TO} ($\mathbf{q}=\mathbf{0}$) across the $B3\rightarrow B1$ phase transition. The physical mechanism causing this effect originates (i) in the geometry of the sodium-chloride structure and (ii) in the covalent interaction. The softening of the TO mode in ferroelectric materials such as SnTe has the same physical origin.

Since the bond length for a unit cell of given volume is larger in the $B1$ phase than in the $B3$ phase, the overlap interaction ($E_{\text{overlap}}\propto d^{-5}$) is less repulsive in the $B1$ phase. This effect reduces the TO frequency of the $B1$ phase relative to the $B3$ phase, since $M\nu_{\text{TO}}^2\propto d^2E_{\text{overlap}}/du^2\propto d^{-7}$. This reduction amounts to approximately 50% of the calculated softening of ν_{TO} in Table VI.

The calculations show that the relative sublattice displacement associated with ν_{TO} lowers the sum of the valence-band energies in both the $B3$ and $B1$ phase. This effect, which destabilizes ν_{TO}, is theoretically found to be much more pronounced in the $B1$ phase. In ZnTe, for example, the second derivative of the covalent energy is given by $d^2E_{\text{cov}}/du^2=-3.6$ eV Å^{-2} in the $B3$ phase and $=-9.4$ eV Å^{-2} in the $B1$ phase. This destabilization originates in a unique feature of the energy bands in the rocksalt phase. At the L point, the anion p states, which form the upper valence bands, do not couple to the cation p states, which form the lower part of the conduction bands. The displacement u mixes the cation and anion states and pushes them apart. The $\mathbf{k}$ sum over the occupied band energies is found to be dominated by contributions near the L point. To second order in u, the energy change of the valence bands is therefore dominated by terms of the form

$$\Delta E\propto\frac{|\langle vL\,|\,\delta\mathbf{H}_{\text{el}}\cdot\mathbf{u}\,|\,cL\rangle|^2}{E_{vL}-E_{cL}}\,, \tag{5.4}$$

which are all negative. In the $B3$ phase, on the other hand, the energy bands have mixed anion and cation character throughout the Brillouin zone already in the unperturbed lattice. This implies that the displacement causes a particular valence-band state to be pushed by both higher *and* lower states rather than being coherently lowered in energy.

Which materials are likely to have soft TO modes? On the basis of the above arguments, we find two prerequisites for soft phonon modes: (i) the crystal should be in the $B1$-phase and (ii) the difference in the cation and anion atomic energies should be small, as can be seen from Eq. (5.4). The group of IV-VI compounds represents such a class of materials.[102]

In order to check these arguments, we have applied the present theory to a IV-VI compound, namely SnTe.[103] We find the $B1$-phase to be the stable phase at zero pressure with a lattice constant $a=6.51$ Å (experiment:[54] $a=6.32$ Å). The calculations give indeed $\nu_{\text{TO}}^2<0$ which implies a structural instability of the $B1$ phase. This is in qualitative accord with experiment and recent *ab initio* calculations[19] of IV-VI compounds.

F. Summary

Let us summarize the main results of this discussion. In this paper, we have considered cubic, binary *sp*-bonded semiconductors and insulators. The chemical trends in the structural properties of *sp*-bonded solids can be understood entirely in terms of the valence orbital energies of their constituent atoms. It is therefore useful to define an atomic electronegativity difference for a compound AB which one may take as the difference $w_{s,\text{cation}}-w_{p,\text{ anion}}$ between the outermost atomic cation s and anion p orbital energies for heteropolar compounds.

(i) The equilibrium bond length of a crystal increases in any sequence of compounds AB with one type of atoms fixed and the other varying downward in a column of the Periodic Table.

(ii) The bulk modulus decreases with increasing equilibrium volume. For a given volume, it also decreases in a series of compounds with increasing atomic electronegativity differences.

(iii) As a function of pressure, structural phase transformations can occur only in the sequence zinc blende $\rightarrow$rocksalt$\rightarrow$cesium chloride.

(iv) The transition pressures P_t for the $B3\rightarrow B1$ and $B1\rightarrow B2$ transition generally decrease with increasing equilibrium volume. They also decrease in any series of compounds with increasing atomic electronegativity differences. For compounds with the same metal ion the latter trend counteracts the trend with volume and leads to a very weak volume dependence of P_t.

(v) The TO phonons strongly soften across a pressure-

induced phase transition from the zinc blende to the rocksalt phase. This softening is caused by the symmetry of the rocksalt phase and is more pronounced in crystals with a smaller atomic electronegativity difference.

ACKNOWLEDGMENTS

We should like to acknowledge several clarifying discussions with Professor W. Harrison. This work was supported in part by the Fonds zur Förderung der wissenschaftlichen Forschung in Österreich, Project No. P5197, and by the Department of Energy through Contract No. W-7405-Eng-36.

APPENDIX: A TWO-STATE MODEL

In order to illustrate the model developed in Sec. II, we further simplify the Hamiltonian in Eq. (2.3). We include only a single s state on the cation site and three p states on the anion site. In addition, we neglect all transfer-matrix elements except $t_{sp\sigma}$ between nearest neighbors. These assumptions are qualitatively appropriate for a heteropolar solid.

The band-structure energy can be evaluated analytically if the $\mathbf{k}$ sum in Eq. (2.1) is approximated by the Baldereschi point.[104] The cation core charge is denoted by $Z_c=Z$ and the electron occupancy on the cation by $Q_c=Q$. Note that $Q_c+Q_a=6$, since there are three doubly occupied valence bands. In a I-VII compound, one has $Z_c=1$ and $Z_a=5$, since the anion s electrons are included in the core in this simple model. One obtains easily

$$\frac{1}{N}\sum_{n,\mathbf{k}}\varepsilon_{n\mathbf{k}}=5\varepsilon_a+\varepsilon_c-2[\tfrac{1}{4}(\varepsilon_c-\varepsilon_a)^2+n_{\mathrm{NN}}t_{sp\sigma}^2]^{1/2}\ , \tag{A1}$$

$$\varepsilon_c=w_c-(U_c-U_M)(Z-Q)+f_c\ , \tag{A2}$$

$$\varepsilon_a=w_a+(U_a-U_M)(Z-Q)+f_a\ , \tag{A3}$$

$$f_a=-n_{\mathrm{NN}}\eta_{sp\sigma}^2\frac{2}{K(w_c+w_a)}\frac{\hbar^4 r_0}{m^2d^5},\quad f_c=3f_a\ , \tag{A4}$$

$$Q=2R^2/(R^2+T^2),\quad R=1-(1+T^2)^{1/2}\ ,$$
$$T^2=\frac{n_{\mathrm{NN}}t_{sp\sigma}^2}{\frac{1}{4}(\varepsilon_c-\varepsilon_a)^2}\ . \tag{A5}$$

In Eqs. (A1) and (A4), n_{NN} is the number of nearest neighbors. The remaining terms are defined in Sec. II. The electron charge Q is calculated self-consistently with the orbital energies of Eqs. (A2) and (A3). After some algebra one obtains

$$E_{\mathrm{cov}}=(1-Q)(\varepsilon_c-\varepsilon_a)-2[\tfrac{1}{4}(\varepsilon_c-\varepsilon_a)^2+n_{\mathrm{NN}}t_{sp\sigma}^2]^{1/2}\ , \tag{A6}$$

$$E_{\mathrm{overlap}}=Qf_c+(6-Q)f_a\ , \tag{A7}$$

$$E_{\mathrm{transfer}}=-(Z-Q)(w_c-w_a)+\tfrac{1}{2}(Z-Q)^2(U_c+U_a-2U_M)\ . \tag{A8}$$

In the ionic limit, $t\to 0$, both Q and E_{cov} tend to zero. If one additionally omits the overlap term, one obtains the expression for E_{coh} which was recently derived in Ref. 15.

---

*Permanent address.

[1]L. Pauling, *The Nature of the Chemical Bond* (Cornell University Press, New York, 1960).

[2]M. Born and K. Huang, *Dynamical Theory of Crystal Lattices* (Clarendon, Oxford, 1954).

[3]J. C. Phillips, *Bonds and Bands in Semiconductors* (Academic, New York, 1973); J. A. Van Vechten, Phys. Rev. **187**, 1007 (1969).

[4]W. A. Harrison, Phys. Rev. B **23**, 5230 (1981).

[5]For a review, see J. C. Phillips, in *Highlights of Condensed-Matter Theory,* Proceedings of the International School of Physics "Enrico Fermi," Course LXXXIX, Varenna, 1984, edited by F. Bassani, F. Fumi, and M. P. Tosi (North-Holland, Amsterdam, 1985), p. 177.

[6]M. P. Tosi, in *Solid State Physics,* edited by F. Seitz and D. Turnbull (Academic, New York, 1964), Vol. 16, p. 1. (1964).

[7]K. N. Jog, R. K. Singh, and S. P. Sanyal, Phys. Rev. B **31**, 6047 (1985).

[8]R. Narayan and S. Ramaseshan, Phys. Rev. Lett. **42**, 992 (1979) (this paper has been critically examined in Ref. 30); R. S. Narayanan, J. Shankar, H. C. Gupta, and B. B. Tripathi, Phys. Status Solidi B **113**, 339 (1982); Y. K. Vohra, S. J. Duclos, and A. L. Ruoff, Phys. Rev. Lett. **54**, 570 (1985).

[9]J. St. John and A. N. Bloch, Phys. Rev. Lett. **33**, 1095 (1974); A. Zunger, *ibid.* **44**, 582 (1980); P. Villars, J. Less-Common Met. **99**, 33 (1984); D. G. Pettifor, J. Phys. C **19**, 285 (1986).

[10]For a review, see M. L. Cohen, in Ref. 5, *Highlights of Condensed-Matter Theory,* p. 16.

[11]A. R. Mackintosh and O. K. Andersen, in *Electrons at the Fermi Surface,* edited by M. Springford (University Press, Cambridge, 1980), p. 149; H. L. Skriver, *The LMTO Method* (Springer, Berlin, 1984); N. E. Christensen, Phys. Rev. B **32**, 207 (1985); O. K. Anderson, O. Jepsen, and D. Glötzel, in *Highlights of Condensed-Matter Theory,* Ref. 5, p. 59; S. Satpathy, Phys. Rev. B **33**, 8706 (1986).

[12]D. G. Pettifor and R. Podloucky, Phys. Rev. Lett. **53**, 1080 (1984); J. Phys. C **19**, 315 (1986).

[13]O. K. Andersen and O. Jepsen, Phys. Rev. Lett. **53**, 2571 (1984).

[14]J. R. Chelikowski and J. K. Burdett, Phys. Rev. Lett. **56**, 961 (1986); see also J. R. Chelikowski, Phys. Rev. B **33**, 8793 (1986); **34**, 5295 (1986).

[15]W. A. Harrison, Phys. Rev. B **31**, 2121 (1985).

[16]W. A. Harrison, Phys. Rev. B **27**, 3592 (1983).

[17]D. J. Chadi, Phys. Rev. B **29**, 785 (1984), and references cited therein.

[18]J. A. Majewski and P. Vogl, Phys. Rev. Lett. **57**, 1366 (1986); this paper gives a short discussion of the model presented here.

[19]K. M. Rabe and J. D. Joannopoulos, Phys. Rev. B **32**, 2302 (1985).

[20]S. Froyen and M. L. Cohen, Phys. Rev. B **29**, 3770 (1984).

[21]K. J. Chang and M. L. Cohen, Phys. Rev. B **30**, 4774 (1984).

[22]M. T. Yin and M. L. Cohen, Phys. Rev. B **26**, 3259 (1982).

[23]S. Froyen and M. L. Cohen, Phys. Rev. B **28**, 3258 (1983).

[24]K. J. Chang and M. L. Cohen, Phys. Rev. B **31**, 7819 (1985).
[25]S. Satpathy, N. E. Christensen, and O. Jepsen, Phys. Rev. B **32**, 6793 (1985).
[26]S. H. Wei and H. Krakauer, Phys. Rev. Lett. **55**, 1200 (1985).
[27]M. Causà, R. Dovesi, C. Pisani, and C. Roetti, Phys. Rev. B **33**, 1308 (1986).
[28]R. Needs and R. M. Martin, Phys. Rev. B **30**, 5390 (1984); K. J. Chang and M. L. Cohen, *ibid.* **31**, 7819 (1985).
[29]C. R. A. Catlow and A. M. Stoneham, J. Phys. C **16**, 4321 (1983).
[30]S. Baroni and A. Baldereschi, J. Phys. Chem. Solids **46**, 675 (1985).
[31]D. R. Jennison and A. B. Kunz, Phys. Rev. B **13**, 5597 (1976).
[32]G. Lucovski, R. M. Martin, and E. Burstein, Phys. Rev. B **4**, 1367 (1971).
[33]C. Muhlhausen and R. G. Gordon, Phys. Rev. B **23**, 900 (1981); **24**, 2147 (1981); **24**, 2161 (1981).
[34]A. J. Cohen and R. G. Gordon, Phys. Rev. B **14**, 4593 (1976).
[35]M. J. Mehl, R. J. Hemley, and L. L. Boyer, Phys. Rev. B **33**, 8685 (1986).
[36]D. Vanderbilt and J. D. Joannopoulos, Phys. Rev. B **22**, 2927 (1980).
[37]For a review, see J. Pollmann, Festkörperprobleme **20**, 117 (1980).
[38]F. Bechstedt, D. Reichardt, and R. Enderlein, Phys. Status Solidi B **131**, 643 (1985).
[39]W. A. Harrison, *Electronic Structure and the Properties of Solids* (Freeman, San Francisco, 1980).
[40]D. J. Chadi and M. L. Cohen, Phys. Status Solidi B **68**, 405 (1975).
[41]G. K. Straub and W. A. Harrison, Phys. Rev. B **31**, 7668 (1985).
[42]P. Vogl, H. P. Hjalmarson, and J. D. Dow, J. Phys. Chem. Solids **44**, 365 (1983).
[43]They are taken from Hartree-Fock calculations of E. Clementi and C. Roetti, At. Data Nucl. Data Tables **14**, 177 (1974). The excited p states were determined from the experimental spectra [C. E. Moore, *Atomic Energy Levels,* (Natl. Bur. Stand. (U.S.) Circ. No. 467 (U.S. GPO, Washington, D.C., 1949)].
[44]W. A. Harrison, Phys. Rev. B **34**, 2787 (1986).
[45]R. Hoffmann, J. Chem. Phys. **39**, 1397 (1963).
[46]A. L. Companion and F. O. Ellison, J. Chem. Phys. **32**, 1132 (1960).
[47]H. J. Monkhorst and J. D. Pack, Phys. Rev. B **13**, 5188 (1976).
[48]L. Ley, R. A. Pollak, F. R. McFeely, S. P. Kowalczyk, and D. A. Shirley, Phys. Rev. B **9**, 600 (1974).
[49]S. T. Pantelides, Phys. Rev. B **11**, 5082 (1975).
[50]R. Haensel, G. Keitel, G. Peters, P. Schreiber, B. Sonntag, and C. Kunz, Phys. Rev. Lett. **23**, 530 (1969).
[51]R. T. Poole, J. G. Jenkin, J. Liesegang, R. C. G. Leckey, Phys. Rev. B **11**, 5179 (1975).
[52]W. Borrmann and P. Fulde, Europhys. Lett. **2**, 471 (1986).
[53]P. B. Gate, Phys. Rev. **139**, A1666 (1965).
[54]R. W. G. Wyckoff, *Crystal Structures,* 2nd ed. (Interscience, New York, 1963).
[55]*Tables Numerical Data and Functional Relationships in Science and Technology,* Vol. 17, Teilen a and b of *Landolt-Bornstein,* edited by O. Madelung, M. Schulz, and H. Weiss (Springer, Heidelberg, 1982).
[56]J. D. Wiley, in *Semiconductors and Semimetals,* edited by R. K. Willardson and A. C. Beer (Academic, New York, 1975), Vol. 10, p. 134.
[57]G. Martinez, in *Handbook of Semiconductors,* edited by M. Balkanski (North-Holland, Amsterdam, 1980), Vol. 2, p. 181.
[58]C. F. Cline, H. L. Dunegan, and G. W. Henderson, J. Appl. Phys. **38**, 1944 (1967).
[59]O. L. Anderson and P. Andreath, Jr., J. Am. Ceram. Soc. **49**, 404 (1966).
[60]V. H. Vetter and R. A. Bartels, J. Phys. Chem. Solids **34**, 1448 (1973).
[61]S. Yamaoka, O. Shimomura, H. Nakazawa, and O. Fukuma, Solid State Commun. **33**, 87 (1980).
[62]O. L. Anderson and J. E. Nafe, J. Geophys. Res. **70**, 3951 (1965).
[63]E. A. Perez-Albuerne and H. G. Drickamer, J. Chem. Phys. **43**, 1381 (1965).
[64]H. G. Zimmer, H. Winzen, and K. Syassen, Phys. Rev. B **32**, 4066 (1985).
[65]A. Jayaraman, B. Batlogg, R. G. Maines, and H. Bach, Phys. Rev. B **26**, 3347 (1982).
[66]M. L. Cohen, Phys. Rev. B **32**, 7988 (1985).
[67]Z. P. Chang and E. K. Graham, J. Phys. Chem. Solids **38**, 1355 (1977).
[68]R. W. Roberts and C. S. Smith, J. Phys. Chem. Solids **31**, 619 (1970); A. J. Darnell and W. A. McCollum, *ibid.* **31**, 805 (1970); S. N. Vaidya and G. C. Kennedy, *ibid.* **32**, 951 (1971); H. Spetzler, C. G. Sammis, and R. J. O'Connell, *ibid.* **33**, 1727 (1972); L. C. Chhabildas and A. L. Ruoff, J. Appl. Phys. **47**, 4182 (1976); Y. Sato-Sorensen, J. Geophys. Res. **88**, 3543 (1983); D. L. Heinz and R. Jeanloz, Phys. Rev. B **30**, 6045 (1984).
[69]C. W. F. T. Pistorius, Prog. Solid State Chem. **11**, 1 (1976).
[70]Heats of formation of the compound from the elements are taken from the *Handbook of Chemistry and Physics* [62nd ed., edited by R. Weast (CRC, Boca Raton, Florida, 1981)], and added to the cohesive energies of the elements from C. Kittel, *Introduction to Solid State Physics,* 3rd ed. (Wiley, New York, 1966).
[71]B. A. Weinstein, Solid State Commun. **24**, 595 (1977).
[72]P. L. Smith and J. E. Martin, Phys. Lett. **19**, 541 (1965).
[73]T. Soma, J. Phys. C **11**, 2669 (1978); *ibid.* **11**, 2681 (1978); T. Soma and H. Matsuo Kaqaya, Solid State Commun. **50**, 261 (1984).
[74]M. B. Owen, P. L. Smith, J. E. Martin, and A. J. Wright, J. Phys. Chem. Solids **24**, 1519 (1963).
[75]A. Jayaraman, W. Klement, Jr., and G. C. Kennedy, Phys. Rev. **130**, 2277 (1963).
[76]C. J. M. Rooymans, Phys. Lett. **4**, 186 (1963).
[77]E. Z. Kaminski, A. V. Omelchenko, and E. I. Estrin, Fiz. Tverd. Tela **12**, 3329 (1970).
[78]R. O. Miller, D. Dachille, and R. Roy, J. Appl. Phys. **37**, 4913 (1966).
[79]S. Ves, K. Strössner, N. E. Christensen, C. K. Kim, and M. Cardona, Solid State Commun. **56**, 479 (1985).
[80]W. Andreoni and K. Maschke, Phys. Rev. B **22**, 4816 (1980).
[81]A. Ohtani, M. Motobayashi, and A. Onodera, Phys. Lett. **75A**, 435 (1980).
[82]N. E. Christensen and O. B. Christensen, Phys. Rev. B **23**, 4739 (1986).
[83]I. Y. Borg and K. D. Smith, J. Phys. Chem. Solids **28**, 49 (1967).
[84]K. Strössner, S. Ves, W. Dieterich, W. Gebhardt, and M. Cardona, Solid State Commun. **56**, 563 (1985).
[85]J. Yamashita and S. Asano, J. Phys. Soc. Jpn. **52**, 3506 (1983).
[86]R. Jeanloz and T. J. Ahrens, Geophys. J. R. Astron. Soc. **62**, 505 (1980); J. F. Mammone, H. K. Mao, and P. M. Bell, Geophys. Res. Lett. **8**, 140 (1981).

[87]Y. Sato and R. Jeanloz, J. Geophys. Res. **86**, 11773 (1981).
[88]L. G. Liu and W. A. Bassett, J. Geophys. Res. **78**, 8470 (1973); the high pressure phase was identified as a PH4I structure which is a distorted cesium chloride structure.
[89]T. A. Grzybowski and A. L. Ruoff, Phys. Rev. B **27**, 6502 (1983).
[90]T. A. Grzybowski and A. L. Ruoff, Phys. Rev. Lett. **53**, 489 (1984).
[91]H. Wendel and R. M. Martin, Phys. Rev. B **19**, 5251 (1979).
[92]A. A. Maradudin, E. W. Montroll, G. H. Weiss, and I. P. Ipatova, *Theory of Lattice Dynamics in the Harmonic Approximation*, 2nd ed. (Academic, New York, 1971).
[93]We performed band-structure calculations for ZnS in the B1 phase, using the empirical pseudopotential method [see M. L. Cohen and V. Heine, Solid State Phys. **24**, 38 (1970)] and find an indirect minimum energy gap of 1.26 eV.
[94]B. A. Weinstein and G. J. Piermanini, Phys. Rev. B **12**, 1172 (1975).
[95]B. N. Harmon, W. Weber, and D. R. Hamman, Phys. Rev. B **25**, 1109 (1982).
[96]R. Trommer, E. Anastassakis, and M. Cardona, in *Light Scattering in Solids*, edited by M. Balkanski, R. C. C. Leite, and S. P. S. Porto (Flammarion, Paris, 1976), p. 396.
[97]K. Kunc and R. M. Martin, in *Ab Initio Calculation of Phonon Spectra*, edited by J. T. Devreese (Plenum, New York, 1983), p. 65.
[98]*International Tables for X-Ray Crystallography*, edited by J. A. Ibers and W. C. Hamilton (Kynoch, Birmingham, 1974), Vol. IV, Sect. 2.
[99]D. R. Yoder and R. Colella, Phys. Rev. B **25**, 2545 (1982).
[100]W. A. Harrison, *Pseudopotentials in the Theory of Metals* (Benjamin, New York, 1966).
[101]The next-nearest-neighbor transfer-matrix elements also contribute to the band width but only to a minor extent (see Sec. IV).
[102]W. Porod and P. Vogl, in *Physics of Narrow Gap Semiconductors*, edited by E. Gornik, H. Heinrich, and L. Palmetshofer (Springer, Berlin, 1982), p. 247.
[103]We have shifted the atomic s-orbital energies slightly downwards by 2.5 eV relative to the p-orbital energies in order to simulate the relativistic increase in the s-p splitting, following Ref. 19.
[104]A. Baldereschi, Phys. Rev. B **7**, 5212 (1973).